Catalysis Communications 172 (2022) 106559

Contents lists available at ScienceDirect

Catalysis Communications

journal homepage: www.elsevier.com/locate/catcom

Novel bimetallic 1%M-Fe/Al_2O_3-Cr_2O_3 (2:1) (M = Ru, Au, Pt, Pd) catalysts for Fischer-Tropsch synthesis

Paweł Mierczyński [a,*], Bartosz Dawid [a], Agnieszka Mierczynska-Vasilev [b], Waldemar Maniukiewicz [a], Izabela Witońska [a], Krasimir Vasilev [c], Malgorzata I. Szynkowska-Jóźwik [a]

[a] Institute of General and Ecological Chemistry, Lodz University of Technology, Zeromskiego 114, 90-543, Lodz, Poland
[b] The Australian Wine Research Institute, Waite Precinct, Hartley Grove cnr Paratoo Road, Urrbrae, Adelaide, SA 5064, Australia
[c] College of Medicine and Public Health, Flinders University, Bedford Park, SA 5042, Australia

ARTICLE INFO

Keywords:
Diesel production
Hydrogenation of CO
Syngas
Iron catalyst
Bimetallic catalysts
Binary oxide

ABSTRACT

The main objective of this work was to study the physicochemical and catalytic properties of bimetallic supported catalysts [1%M-Fe/Al_2O_3-Cr_2O_3 (2:1) (M = Ru, Au, Pt, Pd)] in Fischer-Tropsch synthesis. Furthermore, the study investigated the effect of noble metal addition to iron-supported catalysts on their physicochemical properties and reactivity. The physicochemical properties of the catalysts were studied using a range of characterization techniques such as X-ray diffraction (XRD), temperature-programmed reduction (TPR-H_2), temperature-programmed desorption of ammonia (TPD-NH_3) and BET (Brunauer – Emmett - Teller method). The activity tests were performed by Fischer-Tropsch synthesis in a high-pressure fixed-bed reactor using a gas mixture of H_2 and CO with a molar ratio of 1:1. The correlation between the physicochemical properties of the investigated catalysts and their catalytic performance in CO hydrogenation was also investigated. The reactivity results showed that the most active system exhibited a high specific surface area, the highest total acidity and was the most reducible catalyst compared to the other catalysts tested. In addition, the Au—Fe system showed high selectivity towards liquid product formation during CO hydrogenation.

1. Introduction

Fischer-Tropsch (F-T) synthesis is one of the main alternatives to fossil fuels [1–7]. The advantage of this process is the possibility to obtain clean fuel without sulfur and nitrogen compounds. The wax product obtained during the F-T synthesis can be potentially processed into a diesel or a gasoline fraction [8]. The most well-known catalysts used in F-T reactions are cobalt, ruthenium and iron [9–12]. However, the problem with current F-T catalysts is to achieve high selectivity towards fuel fraction production. Therefore, much effort is put into selecting active phase promoters and support material additives to improve the reactivity of the catalytic material [13,14]. Much attention has recently been paid to the preparation of highly active iron catalysts [15,16]. The improvement of catalyst activity and selectivity is usually achieved by modifying the active phase structure (e.g., exposure of crystal walls, improvement of the metallic dispersion of the active phase, etc.) and changes in the electronic structure of the active phase. It has been shown that the use of ruthenium catalysts in the F-T process for the formation of heavier hydrocarbons does not require any modification. In contrast, iron or cobalt-based catalysts require the introduction of appropriate promoters. It is well known that iron and cobalt-based systems are promoted by alkali metal ions, and noble or transition metal oxides. Usually, iron-supported catalysts are promoted by Ru, which changes the electron properties of these systems [9]. The modification of iron catalysts improves their activity and selectivity. This behaviour is associated with an increase in CO chemisorption while inhibiting hydrogen chemisorption. The increase of the iron catalyst activity in the F-T process is associated with its modification by Ru [6,9,17]. The addition of noble metal facilitates the reducibility of the iron catalyst and may increase the number of carbides formed on its surface. These phenomena can increase the selectivity of the Fe system towards the formation of a gasoline or a diesel fraction. To the best of our knowledge, there is no information in the literature concerning of supported catalysts promoted with noble metals such as Au, Pt, Pd used

* Corresponding author.
E-mail address: pawel.mierczynski@p.lodz.pl (P. Mierczyński).

https://doi.org/10.1016/j.catcom.2022.106559
Received 7 September 2022; Received in revised form 29 October 2022; Accepted 6 November 2022
Available online 7 November 2022

in the Fischer-Tropsch synthesis. Very few information can be found in the literature about the influence of various noble metals addition on selectivity and activity results of iron catalysts supported on the same catalytic carrier. In addition, the lack is the works presenting the comparison studies about bimetallic systems containing noble metal promoters testing in Fischer-Tropsch synthesis. Therefore, the main objective of the present work was to select the most optimal promotor for the catalyst to improve the selectivity of iron catalysts towards the liquid product. Furthermore, the correlation between the catalytic and physicochemical properties of bimetallic supported catalysts was determined.

2. Experimental

2.1. Catalyst and support preparation

Al_2O_3-Cr_2O_3 (2:1) was prepared via co-precipitation method from appropriate aqueous solution of $Al(NO_3)_3{\cdot}9H_2O$ and $Cr(NO_3)_3{\cdot}9H_2O$. An aquas solution of ammonia was used as a precipitating agent during the co-precipitation process. Then the obtained material was calcined for 4 h in air atmosphere at 400 °C. Monometallic iron catalyst Fe/Al_2O_3-Cr_2O_3 (2:1) was prepared by impregnation method using $Fe(NO_3)_3 \cdot 9H_2O$ as an active phase precursor. The obtained catalysts were calcined in an air atmosphere for 4 h at 400 °C. The bimetallic Ru—Fe, Pd—Fe and Pt—Fe catalysts were prepared by subsequent impregnation from the ruthenium (III) chloride, palladium (II) chloride or palladium (II) nitrate and hexachloroplatinic acid solution, respectively. While, the bimetallic Au—Fe catalyst was prepared by deposition – precipitation method according to the procedure described in our previous work [18]. The second bimetallic Pd—Fe catalyst was also prepared via the impregnation method employed previously in synthesizing the Fe/Al_2O_3-Cr_2O_3 (2:1) catalyst but using palladium (II) chloride solution. The metal loading for monometallic iron catalyst was 40 wt% of Fe. While, in the case of bimetallic catalysts 1%M-Fe/Al_2O_3-Cr_2O_3 (2:1) (M = Ru, Au, Pt, Pd) the metal loading was following 40 wt% of Fe and 1 wt% of noble metal.

2.2. Characterization of the catalytic material

The specific surface area (SSA) of the catalytic materials was measured using the BET method [18]. All measurements were performed in a Micromeritics Instrument Corporation, Norcross, GA, USA apparatus. The pore size distributions for catalysts were determined based on the BJH method. The TPD-NH_3 technique was used to investigate the total acidity and the distribution of acid centres present on the catalyst surface. Prior to all TPD runs, 0.2 g of the sample was reduced in situ in a 5%H_2–95%Ar mixture at 500 °C for 1 h and then purified in situ in a He stream at 600 °C for 30 min. Then the catalyst was cooled to ambient temperature in the same atmosphere. In the next step, the physically adsorbed NH_3 was removed from the sample's surface in a helium stream at 100 °C. The chemisorbed ammonia was monitored and recorded using a thermal-conductivity detector (TCD) in each experiment in the temperature range 100–600 °C. Phase composition studies were studied using a PAN analytical Pro MPD using Cu Kα radiation from a sealed tube. A PANalyticalX'Celerator detector was used in all measurements. Reduction studies of the catalytic material was evaluated using the Temperature-programmed reduction technique. TPR-H_2 measurements of catalytic materials were carried out using an automatic AMI-1 instrument in the temperature range 25–900 °C with a linear heating rate of 10 °C/min. In all TPR-H_2 measurements a mixture of 5% H_2_95%Ar was used. A thermal conductivity detector (TCD) was used to monitor the hydrogen concentration. The mass of the sample in each experiment was 0.1 g.

2.3. Catalytic activity measurements in hydrogenation of CO process

The F-T synthesis was carried out in a high-pressure fixed bed reactor using a gas mixture of H_2 and CO with a molar ratio of 1:1. The total flow of the reagents during the reaction was 90 mL•min^{-1}. In each test approximately 2 g of the catalytic material was loaded into the fixed bed high-pressure reactor and the SV at reaction temperature was 7.1 L/g·h (the catalyst bed lenght was 6 mm). The hydrogenation of CO process was carried out at 280 °C under an elevated pressure of 30 bar. Before each test, the catalyst was reduced in situ in a reaction mixture (CO: H_2 = 1) for 1 h at 500 °C. The catalytic activity measurements were done after 20 h of reaction. The conversion of CO and the product concentration formed during the process were determined using chromatographic analysis (GC–MS, GC with TCD, or FID detector). Carbon balance based on the ratio between the molar ratio of all products and the mole of the CO consumed during the catalytic process was calculated.

3. Results and discussion

The catalytic activity data obtained in the Fischer–Tropsch synthesis is given in Table 1. As the results indicate that the distribution of hydrocarbons in the final product depends on the composition of the catalyst used during the Fischer-Tropsch synthesis. The reactivity measurements performed in the hydrogenation of CO showed that the highest CO conversion of 73.7% showed 1%Au-40%Fe/Al_2O_3-Cr_2O_3 (2:1) catalyst. At the same time, the iron catalyst promoted by Pt showed CO conversion of 52.4%. Bimetallic Pd—Fe catalysts prepared using two different precursors, palladium (II) nitrate dihydrate and palladium (II) chloride, were also tested in the F-T process. The Pd—Fe catalyst prepared from the palladium (II) nitrate dihydrate showed higher CO conversion (53.2%) compared to the same system prepared from the palladium (II) chloride precursor (47.4%). On the other hand, bimetallic Ru—Fe catalyst showed the lowest CO conversion value of 27.8%. The results from the catalytic activity studies indicate that in the case of Ru—Fe, Pt—Fe and Au—Fe bimetallic catalysts, CO hydrogenation leads to practically the same number of liquid products in the final product. A slightly lower content of liquid products in the final product was observed for the Pd—Fe catalyst prepared from the palladium (II) chloride precursor. In comparison, the lowest content of liquid hydrocarbon fraction was obtained for the Pd—Fe system prepared from the palladium (II) nitrate dihydrate precursor.

The catalytic activity results showed that the hydrogenation of CO over Ru—Fe catalysts produced the lowest gaseous hydrocarbons content of 28.4%. While in the case of the most active Au—Fe catalyst, the lowest content of CO_2 formed was detected in the effluent gas mixture. This result indicates that during the F-T process using the Au—Fe system, the conversion of monoxide with water vapour (WGS) proceeds only to a small extent. It should also be noted that hydrogenation of CO with Pt—Fe and Au—Fe catalysts leads to approximately the same content of released gaseous hydrocarbons (methane, ethane, propane, and butane) of 33.7 and 33.5%, respectively. On the other hand, the F-T process carried out using bimetallic Pd—Fe synthesized from the palladium (II) chloride and palladium (II) nitrate dihydrate leads to the highest content of gaseous hydrocarbons in the final product of 39.0 and 40.7%, respectively. In addition, the carbon balance for the process conducted over bimetallic catalysts were also calculated and it was inserted in the text of the manuscript. The calculated values showed that in all cases the carbon balance was below 90%. These results confirm the formation of the iron carbides during the conducting the process and may also be assigned with the accuracy of determining the content of the analyzed products. It should be noted that during the analysis of the products and the evaluation of the CO conversion two GC and one GC–MS chromatographs were applied. The analysis of the obtained liquid products was performed using the GC–MS technique. The distribution of the hydrocarbons formed during the hydrogenation of carbon

Table 1
Distribution of products obtained during F–T synthesis carried out on bimetallic supported catalysts.

Catalysts	CO_2 (%)	CH_4 (%)	C_2H_6 (%)	C_3H_8 (%)	C_4H_{10} (%)	Liquid (%)	CO Conv. (%)	Carbon balance (%)
1%Ru-40%Fe/Al_2O_3-Cr_2O_3 (2:1)	6.3	19.5	7.0	1.7	0.2	65.3	27.8	88.9
1%Pd-40%Fe/Al_2O_3-Cr_2O_3 (2:1) (palladium (II) chloride)	3.3	22.3	11.4	4.4	0.9	57.7	47.4	87.4
1%Pt-40%Fe/Al_2O_3-Cr_2O_3 (2:1)	2.8	17.3	9.9	5.3	1.2	63.5	52.4	87.8
1%Au-40%Fe/Al_2O_3-Cr_2O_3 (2:1)	1.7	18.7	8.9	4.6	1.3	64.8	73.7	89.8
1%Pd-40%Fe/Al_2O_3-Cr_2O_3 (2:1) (palladium (II) nitrate dihydrate)	4.2	23.8	9.8	6.0	1.1	55.1	53.2	86.1

monoxide for all bimetallic supported catalysts tested is given in Table 2. Analyses of the liquid products obtained during hydrogenation of CO showed the formation of linear and branched hydrocarbons. The results presented in Table 2 show that when the Pt—Fe catalyst in employed, only linear hydrocarbons are formed. In comparison, when other bimetallic catalysts are used, both linear and branched hydrocarbons are formed. In the case of Pd—Fe catalysts prepared from the palladium (II) chloride precursor, the most branched hydrocarbons were formed. Furthermore, the lowest content (5.2%) of branched hydrocarbons were formed for the bimetallic 1%Ru-Fe/Al_2O_3-Cr_2O_3 catalyst. For the most active Au—Fe catalyst, 8.9% of branched hydrocarbons were detected in the liquid product.

The hydrocarbons formed in the liquid product were analyzed for their respective gasoline and diesel fractions. The partitioning of the liquid product into a gasoline fraction (C_5-C_9) and a diesel fraction (C_{10}-C_{21}) in the CO hydrogenation process is given in Table 3. The GC–MS analysis showed that both C_5-C_9 and C_{10}-C_{21} hydrocarbons are formed for all catalytic systems tested. It should be emphasized that in the case of the Pt—Fe and Pd—Fe catalysts formed from chloride precursor, the highest amount of diesel fraction was formed. In the case of bimetallic Au—Fe catalysts, 41.6% gasoline fraction and 58.4% diesel fraction were formed. However, the largest gasoline fraction was formed for the bimetallic Ru—Fe catalyst, which was also characterized by the highest CO_2 content in the gaseous products.

Table 4 presents the comparison of the catalytic results of the investigated bimetallic catalysts with other systems used in F-T process. The results clearly showed that bimetallic catalysts except of Ru—Fe system exhibited high CO conversion values at lower temperature (280 °C) compared to the rest systems presented in the Table 4. In addition, they also showed high selectivity towards C_{5+} hydrocarbons production what is beneficial from the application point of view of their uses in fuel fractions production. The prepared bimetallic catalytic systems showed also low CO_2 and C_2-C_4 selectivity in the studied reaction.

To understand the activity of the bimetallic iron supported catalyst in the Fischer–Tropsch synthesis, specific surface area (SSA) measurements were performed. The SSA results obtained for the bimetallic iron catalysts are presented in Table 5 and Fig. 1. The pore size distributions showed that the most active 1%Au - 40%Fe/Al_2O_3–Cr_2O_3 (2:1) system had the smallest average pore radius of about 3.5 nm. It also showed the highest specific surface area of 130 $m^2 \cdot g^{-1}$. The same average pore radius of 3.5 nm was measured for the Pd—Fe catalyst prepared using palladium (II) nitrate dihydrate. This system also exhibited a high SSA of 124.2 $m^2 \cdot g^{-1}$. While the less active 1%Pt - 40%Fe/Al_2O_3–Cr_2O_3 (2:1) and 1%Pd-40%Fe/Al_2O_3–Cr_2O_3 (2:1) catalysts (prepared from the palladium (II) chloride precursor) exhibited the same average pore radius of 3.7 nm and the SSA values of 113 and 119 $m^2 \cdot g^{-1}$, respectively. The ruthenium-promoted iron catalyst had the lowest SSA and the highest average pore radius of 4.2 nm, showing the lowest CO conversion in CO hydrogenation.

Table 2
Distribution of hydrocarbon fractions in the liquid product formed on bimetallic supported catalysts in Fischer - Tropsch synthesis.

Hydrocarbon fraction	1%Pd	1%Pt	1%Au	1%Ru
Linear hydrocarbons (%)	90.3	100.0	91.1	94.8
Branched hydrocarbons (%)	9.7	0.0	8.9	5.2
Unsaturated hydrocarbons (%)	0.0	0.0	0.0	0.0

Table 3
Distribution of liquid hydrocarbons formed using 1%M-Fe/Al_2O_3-Cr_2O_3 bimetallic catalysts (where M = 1%Au, 1%Ru, 1%Pt or 1%Pd) in the Fischer - Tropsch synthesis determined using GC–MS.

Hydrocarbon fraction	1%Pd	1%Pt	1%Au	1%Ru
C_5-C_9 (%)	21.1	27.6	41.6	73.7
C_{10}-C_{21} (%)	78.9	72.4	58.4	26.3

To investigate the interaction between the catalyst components, their reducibility was determined using the TPR-H_2 technique. The reduction profiles recorded for bimetallic iron containing catalysts are shown in Fig. 2. To better understand the observed reduction steps, TPR–H_2 measurement recorded for monometallic Fe catalyst was also included. The TPR profile recorded for the 40%Fe/Al_2O_3-Cr_2O_3 catalyst showed three reduction stages with maxima of the hydrogen consumption peaks at 230, 350 and 500 °C, respectively. The first reduction stage (in the temperature range 240-260 °C) is associated with the reduction of Fe_2O_3 to Fe_3O_4. The second reduction peak (~260 °C) is attributed to the reduction of Fe_3O_4 to metallic Fe. The third reduction peak (between 450 °C and 550 °C) relates to the reduction of the spinel phase (iron aluminate or iron chromite) to metallic iron [23,24]. The reduction of iron oxides has been extensively studied by Jóźwiak et al. [24]. The authors proposed a two- or three-stage mechanism for hematite reduction. They found that hematite reduction proceeds according to the following scheme: $Fe_2O_3 > Fe_3O_4 > Fe$. These authors also found that when the temperature of total reduction of iron oxides exceeds 570 °C, hematite is reduced in three reduction steps according to the following scheme: $Fe_2O_3 > Fe_3O_4 > FeO > Fe$.

Furthermore, they also established that depending on the process conditions, the complete reduction of hematite to metallic iron can be achieved at low temperatures, up to 380 °C, in an atmosphere of pure hydrogen [23]. The physicochemical properties of spinel supported catalytic systems have also been studied [23,25]. The authors studied the reducibility of $FeAlO_3$ system using the TPR-H_2 method. Three reduction effects were observed, corresponding to the reduction of iron oxide forms, which proceed in parallel with the reduction of the spinel structure system. The following two schemes can describe the reduction mechanism of the $FeAlO_3$ binary oxide:

$$Fe_2O_3 \Rightarrow Fe_3O_4 \Rightarrow Fe \text{ and/or}$$

$$FeAlO_3 \Rightarrow Fe_2AlO_4 \Rightarrow FeAl_2O_4 \Rightarrow Fe$$

The first mechanism is the reduction of hematite. The second mechanism represents the reduction of the $FeAlO_3$ binary oxide through spinel structure reduction steps, leading to the final product - metallic iron and iron (II) aluminate $FeAl_2O_4$ which is difficult to reduce up to 900 °C in an atmosphere of 5% H_2–95% Ar.

TPR - H_2 profiles recorded for bimetallic 1% Pt-40% Fe/Al_2O_3-Cr_2O_3 (2: 1) and 1% Pd-40% Fe/Al_2O_3-Cr_2O_3 (2: 1) catalysts prepared using

Table 4
The catalytic activity results of Fe-based catalysts in Fischer-Tropsch synthesis.

Catalyst	Metal Loading (%)	SV	H_2/CO	P (Bar)	Temp (°C)	CO_2 (%)	Hydrogen selectivity (%)				CO conv. (%)	Ref.
							CH_4 (%)	**C_2-C_4 (%)**	**C_2-$C_4^=$ (%)**	**C_{5+} (%)**		
Fe/SiO_2	20%	3.6 L/g·h	1.0	10.0	350	15.0	24.0	5.0	31.0	40.0	11.0	[19]
Au-Fe/Al_2O_3-Cr_2O_3	1%Au-40% Fe	7.1 L/g·h	1.0	30.0	280	1.7	18.7	14.8[a]	–	64.8	73.7	This work
Pt-Fe/Al_2O_3-Cr_2O_3	1%Pt-40%Fe	7.1 L/g·h	1.0	30.0	280	2.8	17.3	16.4[a]	–	63.5	52.4	This work
Pd-Fe/Al_2O_3-Cr_2O_3 Palladium (II) chloride	1%Pd-40% Fe	7.1 L/g·h	1.0	30.0	280	3.3	22.3	16.7[a]	–	57.7	47.4	This work
Ru-Fe/Al_2O_3-Cr_2O_3	1%Ru-40% Fe	7.1 L/g·h	1.0	30.0	280	6.3	19.5	8.9[a]	–	65.3	27.8	This work
Pd-Fe/Al_2O_3-Cr_2O_3 Palladium (II) nitrate dihydrate	1%Pd-40% Fe	7.1 L/g·h	1.0	30.0	280	4.2	23.8	16.9[a]	–	55.1	53.2	This work
$FeSn/SiO_2$ (m)	10%Fe	3.6 L/g·h	1.0	10.0	350	26.0	28.0	6.0	33.0	33.0	8.0	[19]
$FeSb/SiO_2$ (m)	10%Fe	3.6 L/g·h	1.0	10.0	350	24.0	18.0	5.0	24.0	53.0	14.0	[19]
$Fe/2\%K_2O/83\%ZnAl_8O_{13}$	15%Fe	1.5 L/g·h	1.0	20.0	340	69.1	18.7	67.4	58.6	13.9	1.7	[20]
$Fe/2\%K_2O/83\%ZnAl_2O_4$	15%Fe	1.5 L/g·h	1.0	20.0	340	17.6	15.4	17.6	14.3	67.0	6.7	[20]
Fe/SBA-15	10%Fe	16.0 L/g·h	2.1	20.0	300	10.2	21.0	20.9	14.3	43.8	24.7	[16]
Fe/AC	10%Fe	16.0 L/g·h	2.1	20.0	300	34.1	7.8	17.3	21.2	53.7	64.0	[16]
Fe/SiO_2	10%Fe	8.0 L/g·h	2.1	20.0	300	19.1	14.6	17.4	20.2	47.8	38.8	[16]
Fe	100Fe*	7.0 L/g·h	2.0	30.0	270	6.0	18.2	39.8a	–	42.0	29.4	[21]
Fe/B	100Fe/1.22B*	7.0 L/g·h	2.0	30.0	270	4.5	21.4	36.1a	–	42.5	30.8	[21]
Fe/B	100Fe/3.70B*	7.0 L/g·h	2.0	30.0	270	5.4	19.7	33.9a	–	46.4	32.1	[21]
Fe-H-M	5%	13.5 L/g·h	2.0	20.7	300	21.3	36.8	30.2a	–	11.7	14.4	[22]
Fe-Na-M	5%	13.5 L/g·h	2.0	20.7	300	12.9	47.8	27.8a	–	11.5	7.3	[22]

* - the numbers present the atomic ratio derived from Induced Coupled Plasma-Optical Emission Spectrometry measurements.
[a] - all content of C_2-C_4 hydrocarbons (olefin and paraffin).

Table 5
Specific surface area and average pore radius for iron catalyst supports.

Catalyst	Specific surface area (m^2g^{-1})	Average pore radius (nm)
1%Ru-40%Fe/Al_2O_3-Cr_2O_3 (2:1)	100	4.2
1%Pd-40%Fe/Al_2O_3-Cr_2O_3 (2:1) palladium (II) chloride	119	3.7
1%Pt-40%Fe/Al_2O_3-Cr_2O_3 (2:1)	113	3.7
1%Au-40%Fe/Al_2O_3-Cr_2O_3 (2:1)	130	3.5
1%Pd-40%Fe/Al_2O_3-Cr_2O_3 (2:1) palladium (II) nitrate dihydrate	124	3.5

palladium (II) chloride also showed three reduction stages. The first stage occurs in the temperature range of 300–350 °C. The second reduction maximum occurs at 420 °C. The last one, with maximum hydrogen consumption, occurs at 500 °C. While the first reduction stage is related to the reduction of Fe_2O_3 to Fe_3O_4, the second reduction stage is the reduction of magnetite to metallic iron. On the other hand, the third reduction effect, observed in the TPR-H_2 curves at the maximum reduction temperature of 500 °C, is related to the reduction of spinel-structured phases formed during the preparation of the catalytic material. Jin-Yong et al. [26] studied the effect of platinum addition on the reducibility of Fe-Ba/Al_2O_3 catalysts. The authors reported that the addition of platinum to the iron catalyst shifted the iron oxide reduction effects towards lower temperatures due to the spillover effect generated by Pt.

The TPR - H_2 profile recorded for the 1% Au-40% Fe/Al_2O_3-Cr_2O_3 (2: 1) catalyst also showed three reduction stages. The first one, with the maximum hydrogen consumption at 260 °C, is related to the reduction of Fe_2O_3 to Fe_3O_4. With a maximum temperature of 430 °C, the second stage presents the reduction of magnetite to metallic iron. The last reduction stage, observed at about 550 °C, is associated with the reduction of spinel phases formed at the stage of the catalyst preparation [5,23,27]. The TPR - H_2 profile recorded for the 1% Ru-40% Fe / Al_2O_3-Cr_2O_3 (2: 1) catalyst showed four reductions stages. The first two stages are related to the reduction of RuO_2, which takes place in two stages [28]. The apparent reduction effect at 180–350 °C is also associated with the reduction of hematite to magnetite [23]. The last reduction peak at 400–600 °C indicates the reduction of magnetite to metallic Fe. Tengku et al. [29] studied the effect of noble metals, such as Ru, on the reducibility of iron catalysts. They confirmed the promoting effect of ruthenium addition on the reducibility of iron oxides, which was established by shifting the reduction effects towards lower temperatures after introducing 3 wt% of ruthenium into the catalytic system. The work of Witońska et al. [30] also demonstrated that the addition of palladium on the surface of the Fe/SiO_2 iron catalyst facilitates the reduction of the oxidized forms of iron.

In the next stage of this work, the donor-acceptor properties of the bimetallic catalysts were evaluated using the TPD-NH_3 technique. The temperature-programmed desorption of ammonia was used to determine the acidity and the acid centers distribution on the catalyst surface. The distribution of acid centers was calculated from the area under the peaks in the corresponding temperature range. These results are given in Table 6. The TPD-NH_3 results confirmed the presence of three types of acid centers, namely, weak acid, moderately strong and strong acidic. The results obtained for the supported iron-containing catalysts show that the 1%Au-40%Fe/Al_2O_3-Cr_2O_3 catalyst had the highest total acidity compared to the other materials tested. In contrast, the Ru—Fe and Pt—Fe bimetallic systems had the lowest total acidity. Moreover, the palladium catalysts synthesized from palladium (II) chloride and palladium (II) nitrate dihydrate had practically equal values for total acidity of 0.40 and 0.44 $mmol \cdot g^{-1}$.

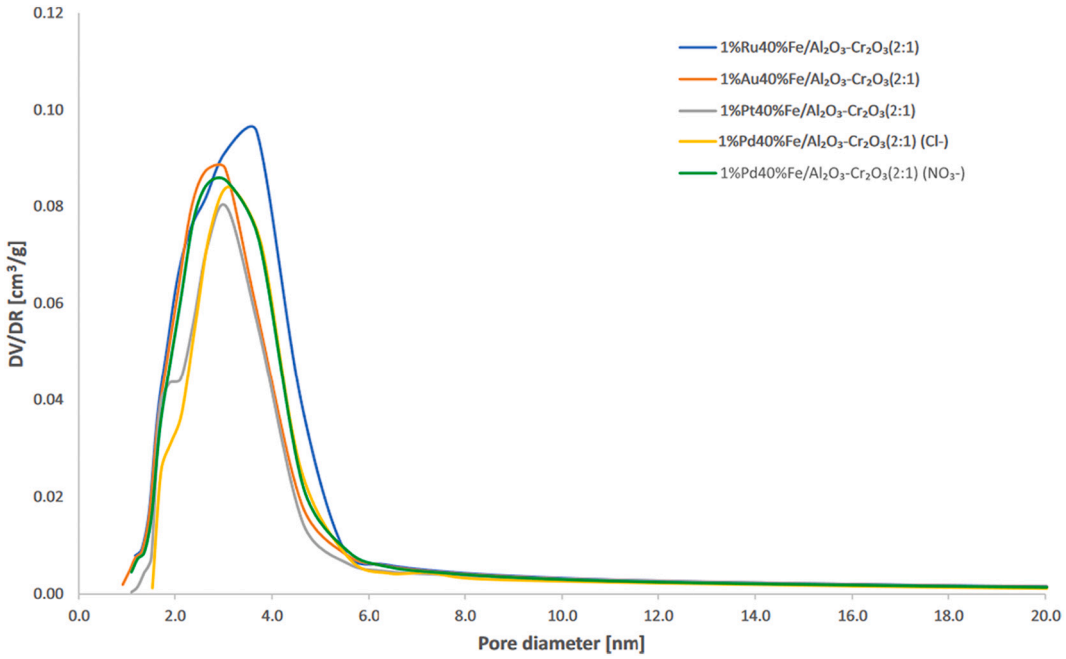

Fig. 1. Pore size distributions of bimetallic noble metal-iron catalysts supported on binary oxide.

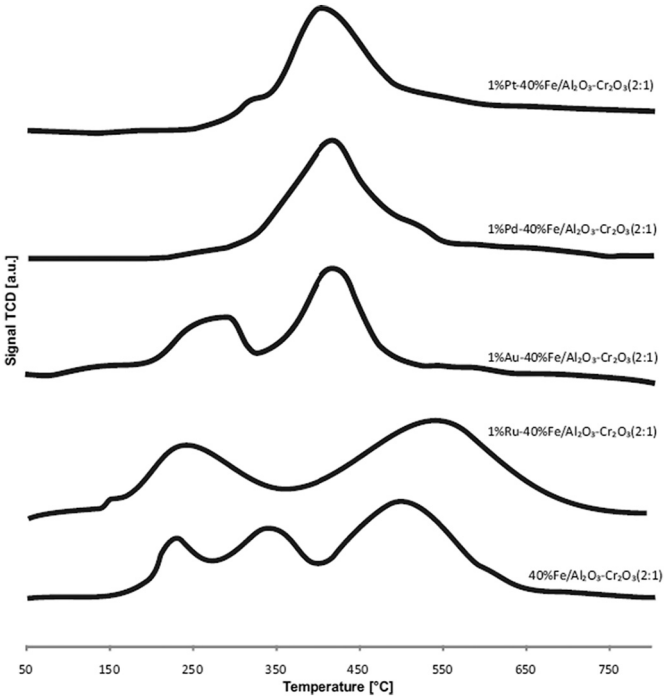

Fig. 2. TPR–H_2 profiles recorded for monometallic and bimetallic Pd—Fe (catalyst prepared from the palladium II chloride precursor), Pt—Fe, Au—Fe and Ru—Fe catalysts supported on Al_2O_3 –Cr_2O_3 (2:1) system.

Table 6
The amount of NH_3 desorbed from the surface of the 1%M-40%Fe/Al_2O_3–Cr_2O_3 (2:1) bimetallic catalysts tested over a range of relevant temperatures.

Catalysts	Weak centers (mmol·g^{-1}) 100–300 °C	Medium centers (mmol·g^{-1}) 300–450 °C	Strong centers (mmol·g^{-1}) 450–600 °C	The total amount of desorbed NH_3 (mmol·g^{-1}) 100–600 °C
1%Ru - 40%Fe/ Al_2O_3 Cr_2O_3 (2:1)	0.09	0.11	0.14	0.34
1%Pd - 40%Fe/ Al_2O_3-Cr_2O_3 (2:1) Palladium (II) chloride	0.12	0.14	0.14	0.40
1%Pt - 40%Fe/ Al_2O_3-Cr_2O_3 (2:1)	0.09	0.11	0.14	0.34
1%Au - 40%Fe/ Al_2O_3-Cr_2O_3 (2:1)	0.18	0.25	0.09	0.62
1%Pd - 40%Fe/ Al_2O_3-Cr_2O_3 (2:1) Palladium (II) nitrate dihydrate	0.13	0.14	0.17	0.44

TPD-NH_3 measurements showed that the most active catalysts also had the highest content of weak centers on their surface, equal to 0.18 mmol·g^{-1} and the highest total acidity compared to the rest of the investigated catalysts. In addition, the catalytic activity results showed that the system which exhibited the highest content of weak acid centers on the catalyst surface like Au—Fe and Pd—Fe catalysts also showed the highest concentration of branched hydrocarbons in the final product. While Pt—Fe catalyst did not show branched hydrocarbons production during the F-T process. This result could explain the high activity of this system in the F-T process. Other authors reported that the selectivity towards C_2-C_4 hydrocarbons formation and the yield towards olefins production decreased with an increase of the total acidity of the investigated systems [31]. The weak acid sites are responsible for the olefin cracking to improve C_2-C_4 olefin selectivity. While the presence of the strong acid sites on the surface leads to C_{5+} fraction production via isomerization and oligomerization. In addition, strong acid sites are also responsible for the enhanced the concentration of isomers and aromatics in the C_{20+} compounds.

In addition, it should be emphasized that the acidity of the catalytic system is a function of the catalysts composition. Our results showed that the calcined and activated and tested systems showed different phase compositions (see XRD studies). These facts confirm that the

activity may be changed during the process until the catalyst phase composition will not change. In our paper we present the activity results for the catalytic systems evaluated after 20 h of the conducting of the process. Based on the results previously presented in our paper [5] we can conclude that the tested system in the presented paper are stable.

To further investigate the activity of the bimetallic catalysts, their phase composition after calcination and after the reaction were measured by XRD. The XRD results are given in Figs. 3 and 4. Diffraction curves recorded for the bimetallic catalysts calcined in air for 4 h at 500 °C indicate the formation of oxidic phases such as hematite and spinel structures (iron aluminate and iron chromite). Any other oxide phases attributable to noble metal oxides were not detected by the XRD technique, or the XRD detection limit was too low to account for the size of the crystallites assigned to these phases.

In the case of the bimetallic catalysts evaluated in the F-T process, the recorded XRD diffractograms showed the following crystallographic phases: γ-Al_2O_3, Fe_3O_4, Fe_2O_3, η-Fe_2C, o-Fe_3C, h-Fe_3C, χ-Fe_5C_2, $FeAl_2O_4$ and $FeCr_2O_4$ (see Fig. 4). It is well known that iron carbides form on the catalyst surface during the activation process performed in a reaction mixture at 500 °C for an hour. During the preparation of the bimetallic catalysts, spinel phases such as iron aluminate and iron chromite are also formed. Moreover, in the case of the Pt—Fe catalyst, additional reflexes attributable to the crystallographic phase of the $Al_{1.9}Cr_{0.1}O_3$ solid solution can be easily recognized. Probably the presence of platinum facilitates the formation of the solid solution during activation and reaction process. Wang et al. [32] studied the effects of various oxide on the carbothermic reduction of synthetic $FeCr_2O_4$. The authors observed that during high temperature reduction of $FeCr_2O_4$, when the reduction degree is higher than 30% an addition of Al_2O_3 significantly affects on reduction behaviour of iron chromite. The phase composition studies of the investigated material showed that next to Al_2O_3, Fe—Cr and solid solution between aluminium (Al_2O_3) and chromium oxides (Cr_2O_3) phases were detected. The authors reported also that Al^{3+} ions can diffuse to the inner core and replace of Cr^{3+} in its structure. The occurrence of the solid solution phase can further explain the lower CO conversion value compared to the activity of the bimetallic Au—Fe system tested in the F-T process. The catalytic activity results and our previous studies have showed that the created carbides are crucial for improving the catalytic activity of iron catalysts in the F-T process. Some authors have even reported that the presence of iron carbides on the catalyst surface are more important than iron dispersion to achieve a high activity in hydrogenation of CO. As shown in Fig. 4, the most active catalyst in CO hydrogenation showed the presence of the following iron carbides of η-Fe_2C, o-Fe_3C, h-Fe_3C and χ-Fe_5C_2 on its surface. It is also worth noting that reflexes assigned to all types of spinel structures, namely, Fe_3O_4, $FeAl_2O_4$ and $FeCr_2O_4$ and additional $FeCrO_3$ phase, were detected. The occurrence of carbides phases are in agreement with literature data and our previous studies [6] and explain the high activity of this system in the F-T process. It is also worth to noted that in the case of bimetallic Au—Fe system additional $FeCrO_3$ phase on the XRD diffraction curve was detected and this phase may be responsible for high conversion value observed for this system in the studied process in comparison to the other investigated catalysts. In addition, it should be noted that the possibility of alloys formation between noble metals and Fe (Au—Fe, Ru—Fe, Pd—Fe and Pt—Fe) cannot be ruled out [33,34]. The formation of such alloys may explain high activity and selectivity of bimetallic catalysts towards C_{5+} fraction production. Our XRD studies did not confirm the alloying process between Fe and noble metals due to low concentration of noble metal in each catalyst and the complex composition of the tested systems. Furthermore, the studied systems have high content of iron species which covered surface of the catalyst result in the lack the appearance of the XRD reflexes coming from the alloy phases.

The high activity and selectivity of iron-containing catalysts are well known to be associated with the presence of the Hägg carbide χ-Fe_5C_2 phase on the catalyst surface. In comparison, catalyst deactivation of the Fe systems is related to the formation of the cementite phase θ-Fe_3C [35,36].

SEM-EDS measurements were performed for the bimetallic Au—Fe, Pt—Fe, Ru—Fe and Pd—Fe supported catalysts to determine their morphology and composition. SEM images and EDS spectra acquired for the catalysts are given in Fig. 5. The results confirmed the catalysts' composition. The same elements, namely, Fe, Al, and Cr, were observed on the catalysts' surface in all cases. Except for the bimetallic Au—Fe system, all the catalysts contained chlorine which originated from the precursor salts used during the preparation step. The absence of this element in the Au—Fe system could be due to how gold was introduced onto the catalyst surface. For the gold-iron catalyst, gold was introduced

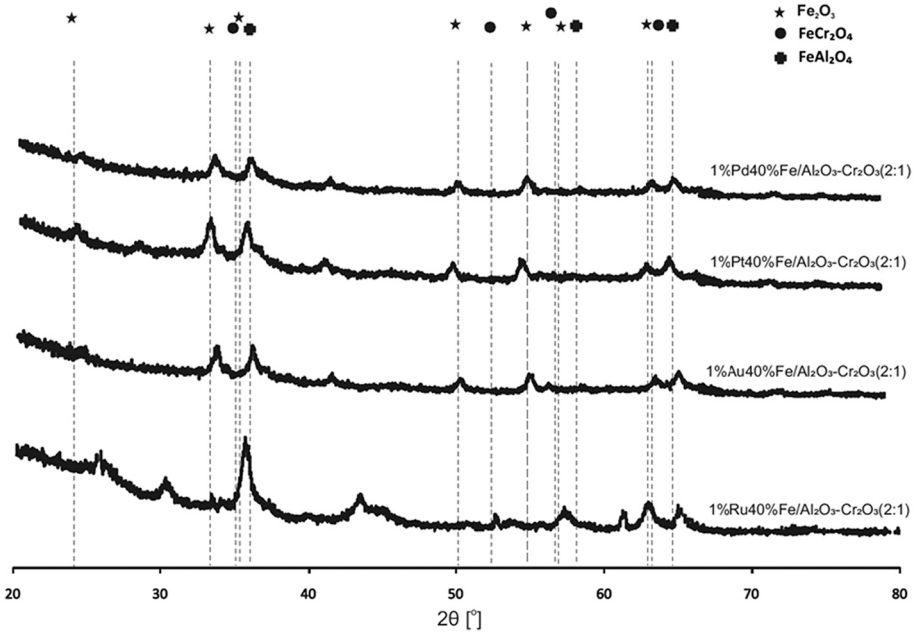

Fig. 3. XRD patterns recorded for the bimetallic Pd—Fe (catalyst prepared from the palladium II chloride precursor), Pt—Fe, Au—Fe and Ru—Fe catalysts supported on Al_2O_3-Cr_2O_3 (2:1) calcined at 400 °C for 4 h in an air atmosphere.

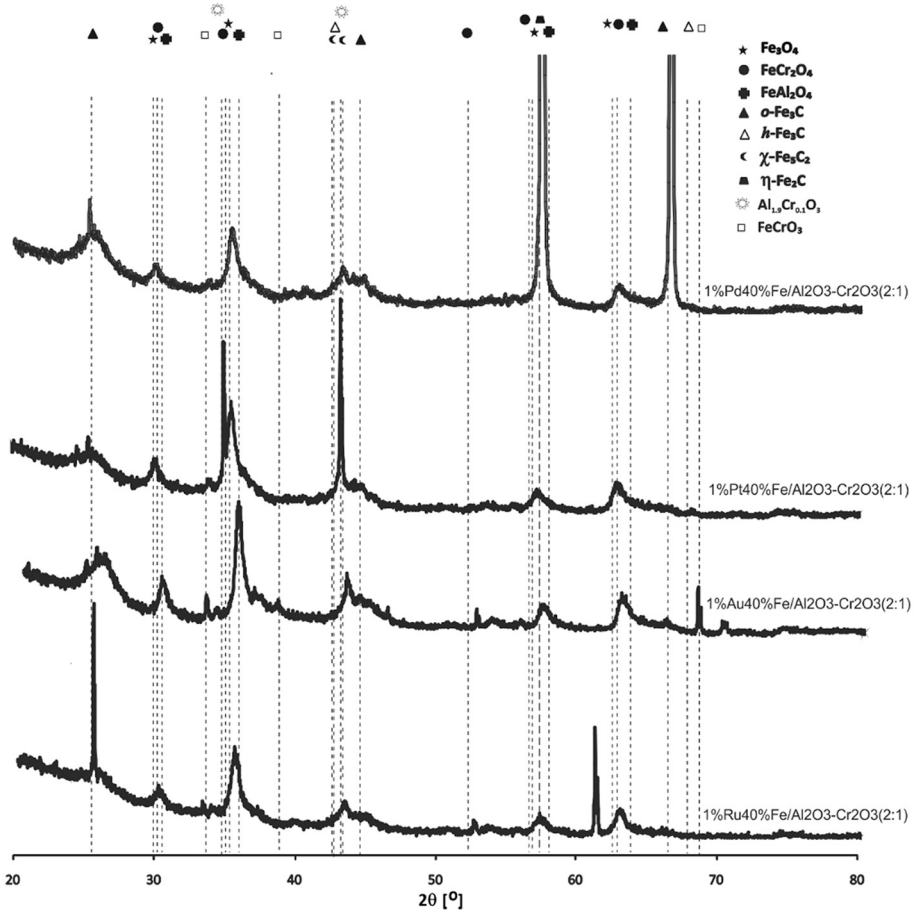

Fig. 4. Diffraction curves recorded for the 1% M-40%Fe/Al_2O_3-Cr_2O_3 (2: 1) bimetallic catalysts (where, M = Pd (catalyst prepared from the palladium II chloride precursor), Pt, Au, Ru) after reduction for 1 h at 500 °C in a 50% H_2–50% CO mixture and reaction.

by the deposition-precipitation method [18]. Furthermore, the SEM images recorded for all catalysts showed that the most active catalysts had the highest distribution of iron species on their surface, which can explain the reactivity results of this system in the F-T process.

4. Conclusions

The catalytic activity of monometallic iron and bimetallic Ru—Fe, Pt—Fe, Au—Fe and Pd—Fe supported catalysts in the F-T process was investigated in detail. The F-T reaction was carried out at 280 °C under elevated pressure (3.0 MPa). The catalyst loading was 2 g and the composition of the reaction mixture used in each catalytic test was: H_2: CO = 1 (molar ratio). The physicochemical properties of the mono and bimetallic supported catalysts were studied using a range of analytical techniques including XRD, BET, TPR, TPD-NH_3 and SEM EDS. The reactivity measurements performed in the studied reaction showed that CO conversion was the highest for bimetallic catalysts on Au—Fe support, leading to the formation of a large amount of liquid product. The catalytic activity of the investigated bimetallic supported catalysts in the F-T reaction can be expressed by the following activity series: Au-Fe > Pt-Fe > Pd-Fe > Ru-Fe. The catalytic activity results provided evidence that the distribution of the hydrocarbons obtained using Ru—Fe, Au—Fe and Pt—Fe bimetallic catalysts had high selectivity towards the formation of liquid products (C_{5+}). However, the Au—Fe and Pd—Fe catalysts exhibited the highest content of branched hydrocarbons in the liquid product. The promotion effect of gold and ruthenium on the catalytic selectivity of iron catalyst towards the formation of liquid products containing C_5 to C_9 carbon atoms was also demonstrated. Furthermore, among all the bimetallic catalysts, the most active system in the F-T process was at the same time also the most easily reducible. It was also confirmed that the carbide phases *o*-Fe_3C, *h*-Fe_3C, χ-Fe_5C_2 and η-Fe_2C had a huge impact on the catalyst activity and selectivity. The reactivity results obtained in Fischer-Tropsch synthesis confirmed that the acidity and phase composition of the catalyst has enormous impact on its catalytic properties. It was shown that the catalyst with the highest total acidity (electron-acceptor properties) exhibited the highest CO conversion and selectivity towards the liquid fraction in F-T synthesis. This system owned the highest content of weak centers on their surface, equal to 0.18 $mmol \cdot g^{-1}$ compared to the rest of the investigated catalysts. In addition, the catalysts which demonstrated the highest content of weak acid centers like Au—Fe and Pd—Fe catalysts also exhibited the highest concentration of branched hydrocarbons in the final product. In addition, the formation of alloy phases between noble metals and Fe cannot be ruled out. The formation of these phases could also explain the high activity and selectivity towards C_{5+} formation in Fischer-Tropsch synthesis. This possibility is confirmed by TPR-H_2 studies, which showed the interaction between Fe and noble metals. The results showed also possible potential application of studied systems in the production of fuel fractions.

CRediT authorship contribution statement

Paweł Mierczyński: Conceptualization, Methodology, Supervision, Visualization, Investigation, Data curation, Writing – original draft, Writing – review & editing, Project administration. **Bartosz Dawid:** Investigation, Data curation. **Agnieszka Mierczynska-Vasilev:** Supervision, Conceptualization, Writing – review & editing. **Waldemar Maniukiewicz:** Investigation. **Izabela Witońska:** Conceptualization,

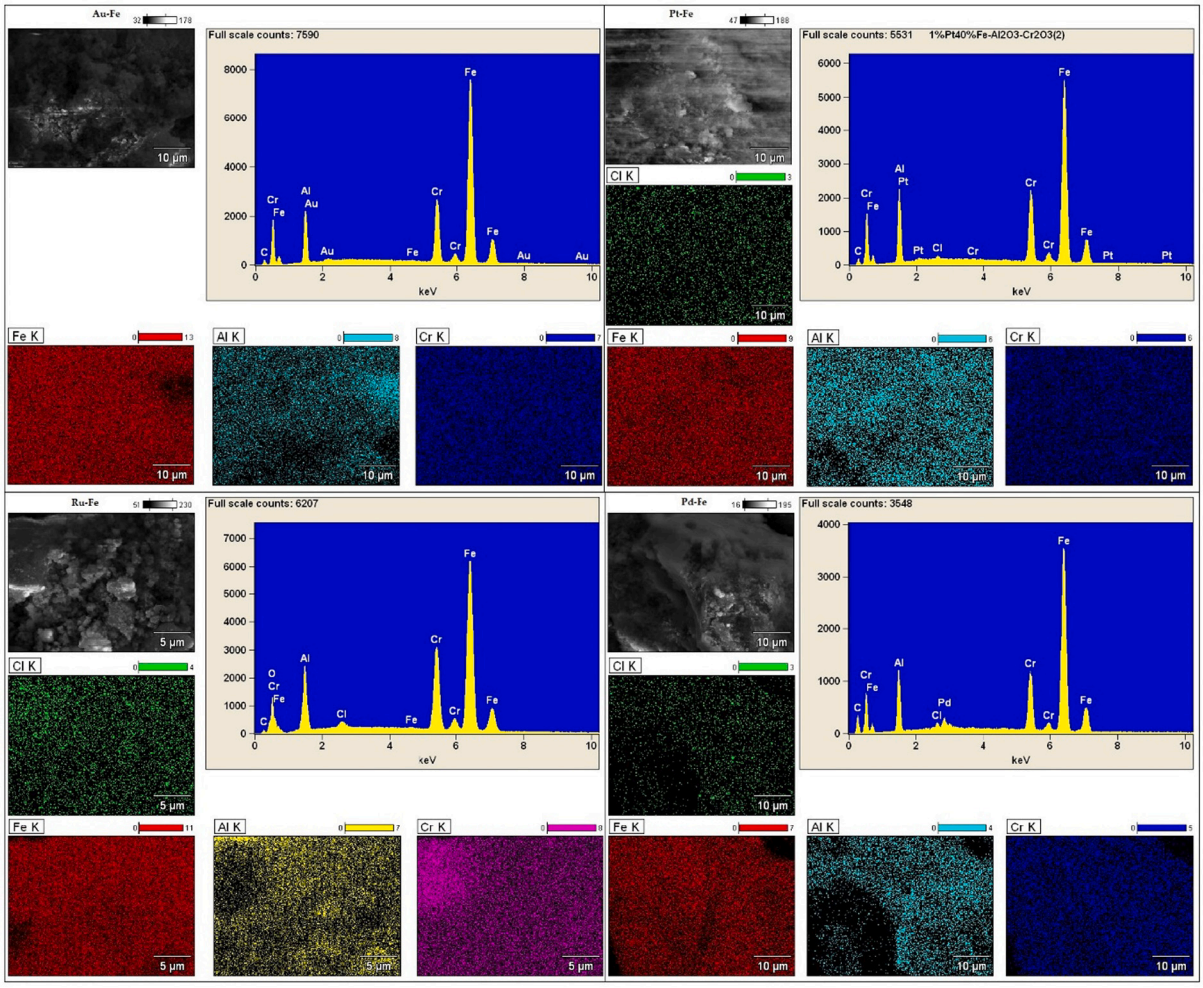

Fig. 5. SEM images and EDS spectra of the investigated materials calcined in air for 4 h at 400 °C.

Funding acquisition. **Krasimir Vasilev:** Supervision, Writing – review & editing. **Malgorzata I. Szynkowska-Jóźwik:** Supervision, Conceptualization.

Declaration of Competing Interest

The authors declare that they have no known competing financial interests or personal relationships that could have appeared to influence the work reported in this paper.

Data availability

Data will be made available on request.

Acknowledgment

This work was partially funded from NCBiR-Grant no. BIO-STRATEG2/297310/13/NCBiR/2016.

References

[1] K.A. Chalupka, W. Maniukiewicz, P. Mierczynski, T. Maniecki, J. Rynkowski, S. Dzwigaj, The catalytic activity of Fe-containing SiBEA zeolites in Fischer–Tropsch synthesis, Catal. Today 257 (Part 1) (2015) 117–121.

[2] P. Mierczynski, B. Dawid, W. Maniukiewicz, M. Mosinska, M. Zakrzewski, R. Ciesielski, A. Kedziora, S. Dubkov, D. Gromov, J. Rogowski, I. Witonska, M. I. Szynkowska, T. Maniecki, Fischer–Tropsch synthesis over various Fe/Al2O3–Cr2O3 catalysts, React. Kinet. Mech. Catal. 124 (2018) 545–561.

[3] R. Sadek, K.A. Chalupka, P. Mierczynski, J. Rynkowski, Y. Millot, L. Valentin, S. Casale, S. Dzwigaj, Fischer-Tropsch reaction on Co-containing microporous and mesoporous Beta zeolite catalysts: the effect of porous size and acidity, Catal. Today 354 (2020) 109–122, https://doi.org/10.1016/j.cattod.2019.05.004. In this issue.

[4] R. Sadek, K.A. Chalupka, P. Mierczynski, J. Rynkowski, J. Gurgul, S. Dzwigaj, Cobalt based catalysts supported on two kinds of beta zeolite for application in fischer-tropsch synthesis, Catalysts 9 (2019).

[5] P. Mierczynski, B. Dawid, K. Chalupka, W. Maniukiewicz, I. Witoska, K. Vasilev, M. I. Szynkowska, Comparative studies of fischer-tropsch synthesis on iron catalysts supported on Al2O3-Cr2O3 (2:1), multi-walled carbon nanotubes or BEA zeolite systems, Catalysts 9 (2019).

[6] P. Mierczynski, B. Dawid, K. Chalupka, W. Maniukiewicz, I. Witonska, M. I. Szynkowska, Role of the activation process on catalytic properties of iron supported catalyst in Fischer-Tropsch synthesis, J. Energy Inst. 93 (2020) 565–580, https://doi.org/10.1016/j.joei.2019.06.008.

[7] K.A. Chalupka, S. Casale, E. Zurawicz, J. Rynkowski, S. Dzwigaj, The remarkable effect of the preparation procedure on the catalytic activity of CoBEA zeolites in the Fischer–Tropsch synthesis, Microporous Mesoporous Mater. 211 (2015) 9–18.

[8] P. Mierczynski, T. Maniecki, J. Kaluzna-Czaplinska, M. Szynkowska, W. Maniukiewicz, M. Lason-Rydel, W. Jozwiak, Hydroconversion of parafine LTP56-H over nickel/Na-mordenite catalysts, Cent. Eur. J. Chem. 11 (2013) 304–312.

[9] M.C. Bahome, L.L. Jewell, K. Padayachy, D. Hildebrandt, D. Glasser, A.K. Datye, N. J. Coville, Fe-Ru small particle bimetallic catalysts supported on carbon nanotubes for use in Fischer–Tröpsch synthesis, Appl. Catal. A Gen. 328 (2007) 243–251.

[10] C. Zhu, G.M. Bollas, Gasoline selective Fischer-Tropsch synthesis in structured bifunctional catalysts, Appl. Catal. B Environ. 235 (2018) 92–102.

[11] J. Zhang, J. Chen, J. Ren, Y. Li, Y. Sun, Support effect of Co/Al2O3 catalysts for Fischer–Tropsch synthesis☆, Fuel 82 (2003) 581–586.

[12] T. Koh, H.M. Koo, T. Yu, B. Lim, J.W. Bae, Roles of ruthenium–support interactions of size-controlled ruthenium nanoparticles for the product distribution of fischer–tropsch synthesis, ACS Catal. 4 (2014) 1054–1060.

[13] J.C. Park, S. Jang, G.B. Rhim, J.H. Lee, H. Choi, H.-D. Jeong, M.H. Youn, D.-W. Lee, K.Y. Koo, S.W. Kang, J.-I. Yang, H.-T. Lee, H. Jung, C.S. Kim, D.H. Chun, A durable

nanocatalyst of potassium-doped iron-carbide/alumina for significant production of linear alpha olefins via Fischer-Tropsch synthesis, Appl. Catal. A Gen. 564 (2018) 190–198.
[14] W.-P. Ma, Y.-L. Zhao, Y.-W. Li, Y.-Y. Xu, J.-L. Zhou, An investigation of chain growth probability in Fischer-Tropsch synthesis over an industrial Fe−Cu−K catalyst, React. Kinet. Catal. Lett. 66 (1999) 217–223.
[15] D. Wang, B. Chen, X. Duan, D. Chen, X. Zhou, Iron-based Fischer–Tropsch synthesis of lower olefins: the nature of χ-Fe5C2 catalyst and why and how to introduce promoters, J. Energy Chem. 25 (2016) 911–916.
[16] K. Cheng, V.V. Ordomsky, M. Virginie, B. Legras, P.A. Chernavskii, V.O. Kazak, C. Cordier, S. Paul, Y. Wang, A.Y. Khodakov, Support effects in high temperature Fischer-Tropsch synthesis on iron catalysts, Appl. Catal. A Gen. 488 (2014) 66–77.
[17] A.J. Barrios, B. Gu, Y. Luo, D.V. Peron, P.A. Chernavskii, M. Virginie, R. Wojcieszak, J.W. Thybaut, V.V. Ordomsky, A.Y. Khodakov, Identification of efficient promoters and selectivity trends in high temperature Fischer-Tropsch synthesis over supported iron catalysts, Appl. Catal. B Environ. 273 (2020), 119028.
[18] P. Mierczynski, K. Vasilev, A. Mierczynska, W. Maniukiewicz, M.I. Szynkowska, T. P. Maniecki, Bimetallic Au-Cu, Au-Ni catalysts supported on MWCNTs for oxy-steam reforming of methanol, Appl. Catal. B Environ. 185 (2016) 281–294, https://doi.org/10.1016/j.apcatb.2015.11.047.
[19] D.V. Peron, A.J. Barrios, A. Taschin, I. Dugulan, C. Marini, G. Gorni, S. Moldovan, S. Koneti, R. Wojcieszak, J.W. Thybaut, M. Virginie, A.Y. Khodakov, Active phases for high temperature Fischer-Tropsch synthesis in the silica supported iron catalysts promoted with antimony and tin, Appl. Catal. B Environ. 292 (2021), 120141.
[20] Z. Liu, G. Jia, C. Zhao, Y. Xing, Selective iron catalysts for direct Fischer–Tropsch synthesis to light olefins, Ind. Eng. Chem. Res. 60 (2021) 6137–6146.
[21] H. Wan, M. Qing, H. Wang, S. Liu, X.-W. Liu, Y. Zhang, H. Gong, L. Li, W. Zhang, C. Song, X.-D. Wen, Y. Yang, Y.-W. Li, Promotive effect of boron oxide on the iron-based catalysts for Fischer-Tropsch synthesis, Fuel 281 (2020), 118714.
[22] R. Liu, Z. Ma, J.D. Sears, M. Juneau, M.L. Neidig, M.D. Porosoff, Identifying correlations in Fischer-Tropsch synthesis and CO2 hydrogenation over Fe-based ZSM-5 catalysts, J. CO2 Utilization 41 (2020), 101290.
[23] W. Jozwiak, T. Maniecki, P. Mierczynski, K. Bawolak, W. Maniukiewicz, Reduction study of Iron-alumina binary oxide Fe2-xAlxO3, Pol. J. Chem. 83 (2009) 2153–2162.
[24] W.K. Jozwiak, E. Kaczmarek, T.P. Maniecki, W. Ignaczak, W. Maniukiewicz, Reduction behavior of iron oxides in hydrogen and carbon monoxide atmospheres, Appl. Catal. A Gen. 326 (2007) 17–27.
[25] T. Maniecki, P. Mierczynski, W. Maniukiewicz, D. Gebauer, W. Jozwiak, The effect of spinel type support FeAlO3, ZnAl2O4, CrAl3O6 on physicochemical properties of Cu, Ag, Au, Ru supported catalysts for methanol synthesis, Kinet. Catal. 50 (2009) 228–234.
[26] J.-Y. Luo, M. Meng, Y.-Q. Zha, Y.-N. Xie, T.-D. Hu, J. Zhang, T. Liu, A comparative study of Pt/Ba/Al2O3 and Pt/Fe-Ba/Al2O3 NSR catalysts: new insights into the interaction of Pt–Ba and the function of Fe, Appl. Catal. B Environ. 78 (2008) 38–52.
[27] L.R. Mentasty, O.F. Gorriz, L.E. Cadus, Chromium oxide supported on different Al2O3 supports: catalytic propane dehydrogenation, Ind. Eng. Chem. Res. 38 (1999) 396–404.
[28] P. Mierczynski, W. Maniukiewicz, T. Maniecki, Comparative studies of Pd, Ru, Ni, Cu/ZnAl2O4 catalysts for the water gas shift reaction (vol 11, pg 912, 2013), Cent. Eur. J. Chem. 11 (6) (2013) 912–919.
[29] T.S.T. Saharuddin, F. Salleh, A. Samsuri, R. Othaman, M.A. Yarmo, Influence of noble metal (Ru, Os and Ag) on the reduction behaviour of iron oxide using carbon monoxide: TPR and kinetic studies, Int. J. Chem. Eng. Appl. 6 (2015) 405.
[30] I.A. Witońska, M.J. Walock, M. Binczarski, M. Lesiak, A.V. Stanishevsky, S. Karski, Pd–Fe/SiO2 and Pd–Fe/Al2O3 catalysts for selective hydrodechlorination of 2,4-dichlorophenol into phenol, J. Mol. Catal. A Chem. 393 (2014) 248–256.
[31] S.-H. Kang, J.W. Bae, P.S. Sai Prasad, S.-J. Park, K.-J. Woo, K.-W. Jun, Effect of preparation method of Fe–based Fischer–Tropsch catalyst on their light olefin production, Catal. Lett. 130 (2009) 630–636.
[32] W. Yaxian, W. Lijun, C. Kuo-Chih, Effects of CaO, MgO, Al2O3 and SiO2 on the carbothermic reduction of synthetic FeCr2O4, J. Min. Metall. Sect. B: Metall. 51 (2015).
[33] H. Fu, M. Li, Q. Xu, G. Chen, Y. Zou, W. Zhang, S. Li, L. Ling, Nitrogen doped carbon-distributed and nitrogen-stabilized ultrafine FeM (M = Pd, Pt, Au) nanoclusters for doxorubicin detoxification, Appl. Catal. B Environ. 316 (2022), 121646.
[34] Y. Sakamoto, K. Higuchi, N. Takahashi, K. Yokota, H. Doi, M. Sugiura, Effect of the addition of Fe on catalytic activities of Pt/Fe/γ-Al2O3 catalyst, Appl. Catal. B Environ. 23 (1999) 159–167.
[35] T. Herranz, S. Rojas, F.J. Pérez-Alonso, M. Ojeda, P. Terreros, J.L.G. Fierro, Carbon oxide hydrogenation over silica-supported iron-based catalysts: influence of the preparation route, Appl. Catal. A Gen. 308 (2006) 19–30.
[36] S. Li, R.J. O'Brien, G.D. Meitzner, H. Hamdeh, B.H. Davis, E. Iglesia, Structural analysis of unpromoted Fe-based Fischer–Tropsch catalysts using X-ray absorption spectroscopy, Appl. Catal. A Gen. 219 (2001) 215–222.